AD

Technical Report ARWSB-TR-11022

Microwave Absorbing Properties of Metallic Glass/Polymer Composites

Stephen Bartolucci

September 2011

ARMAMENT RESEARCH, DEVELOPMENT AND ENGINEERING CENTER
Armaments Engineering & Technology Center
Weapon Systems & Technology

The views, opinions, and/or findings contained in this report are those of the author(s) and should not be construed as an official Department of the Army position, policy, or decision, unless so designated by other documentation.

The citation in this report of the names of commercial firms or commercially available products or services does not constitute official endorsement by or approval of the U.S. Government.

Destroy this report when no longer needed by any method that will prevent disclosure of its contents or reconstruction of the document. Do not return to the originator.

REPORT DOCUMENTATION PAGE

Form Approved
OMB No. 0704-0188

1. REPORT DATE *(DD-MM-YYYY)*	2. REPORT TYPE	3. DATES COVERED *(From - To)*
28-09-2011	Technical	

4. TITLE AND SUBTITLE
Microwave Absorbing Properties of Metallic Glass/Polymer Composites

5a. CONTRACT NUMBER

5b. GRANT NUMBER

5c. PROGRAM ELEMENT NUMBER

6. AUTHOR(S)
Stephen Bartolucci

5d. PROJECT NUMBER

5e. TASK NUMBER

5f. WORK UNIT NUMBER

7. PERFORMING ORGANIZATION NAME(S) AND ADDRESS(ES)
U.S. Army ARDEC
Benet Laboratories, RDAR-WSB
Watervliet, NY 12189-4000

8. PERFORMING ORGANIZATION REPORT NUMBER
ARWSB-TR-11022

9. SPONSORING/MONITORING AGENCY NAME(S) AND ADDRESS(ES)
U.S. Army ARDEC
Benet Laboratories, RDAR-WSB
Watervliet, NY 12189-4000

10. SPONSOR/MONITOR'S ACRONYM(S)

11. SPONSORING/MONITORING AGENCY REPORT NUMBER

12. DISTRIBUTION AVAILABILITY STATEMENT
Approved for public release; distribution is unlimited.

13. SUPPLEMENTARY NOTES

14. ABSTRACT
In this study, the microwave absorption characteristics of metallic glass / polymer composites were investigated. Electromagnetic wave absorption properties in the microwave spectrum are of particular importance to military applications. Radar absorbing materials have been studied for years and are of strategic importance for stealth technology. This work examined high magnetic permeability cobalt-based metallic glasses dispersed in epoxy matrices and measured the reflection loss behavior of the composites in the C-band and X-band spectrum. Results have shown that the metallic glass composites have good absorption in the region of interest due to the absorption properties of the glass particles and the graded structure of the composite.

15. SUBJECT TERMS
Microwave absorption, metallic glass, polymer composites, electromagnetic wave absorption, c-band spectrum, and x-band spectrum.

16. SECURITY CLASSIFICATION OF:			17. LIMITATION OF ABSTRACT	18. NUMBER OF PAGES	19a. NAME OF RESPONSIBLE PERSON
a. REPORT	b. ABSTRACT	c. THIS PAGE	.U	24	Stephen Bartolucci
U/U	U	U			19b. TELEPONE NUMBER (*Include area code*) (518) 266-5189

INSTRUCTIONS FOR COMPLETING SF 298

1. REPORT DATE. Full publication date, including day, month, if available. Must cite at lest the year and be Year 2000 compliant, e.g., 30-06-1998; xx-08-1998; xx-xx-1998.

2. REPORT TYPE. State the type of report, such as final, technical, interim, memorandum, master's thesis, progress, quarterly, research, special, group study, etc.

3. DATES COVERED. Indicate the time during which the work was performed and the report was written, e.g., Jun 1997 - Jun 1998; 1-10 Jun 1996; May - Nov 1998; Nov 1998.

4. TITLE. Enter title and subtitle with volume number and part number, if applicable. On classified documents, enter the title classification in parentheses.

5a. CONTRACT NUMBER. Enter all contract numbers as they appear in the report, e.g. F33615-86-C-5169.

5b. GRANT NUMBER. Enter all grant numbers as they appear in the report, e.g. 1F665702D1257.

5c. PROGRAM ELEMENT NUMBER. Enter all program element numbers as they appear in the report, e.g. AFOSR-82-1234.

5d. PROJECT NUMBER. Enter al project numbers as they appear in the report, e.g. 1F665702D1257; ILIR.

5e. TASK NUMBER. Enter all task numbers as they appear in the report, e.g. 05; RF0330201; T4112.

5f. WORK UNIT NUMBER. Enter all work unit numbers as they appear in the report, e.g. 001; AFAPL30480105.

6. AUTHOR(S). Enter name(s) of person(s) responsible for writing the report, performing the research, or credited with the content of the report. The form of entry is the last name, first name, middle initial, and additional qualifiers separated by commas, e.g. Smith, Richard, Jr.

7. PERFORMING ORGANIZATION NAME(S) AND ADDRESS(ES). Self-explanatory.

8. PERFORMING ORGANIZATION REPORT NUMBER. Enter all unique alphanumeric report numbers assigned by the performing organization, e.g. BRL-1234; AFWL-TR-85-4017-Vol-21-PT-2.

9. SPONSORING/MONITORS AGENCY NAME(S) AND ADDRESS(ES). Enter the name and address of the organization(s) financially responsible for and monitoring the work.

10. SPONSOR/MONITOR'S ACRONYM(S). Enter, if available, e.g. BRL, ARDEC, NADC.

11. SPONSOR/MONITOR'S REPORT NUMBER(S). Enter report number as assigned by the sponsoring/ monitoring agency, if available, e.g. BRL-TR-829; -215.

12. DISTRIBUTION/AVAILABILITY STATEMENT. Use agency-mandated availability statements to indicate the public availability or distribution limitations of the report. If additional limitations/restrictions or special markings are indicated, follow agency authorization procedures, e.g. RD/FRD, PROPIN, ITAR, etc. Include copyright information.

13. SUPPLEMENTARY NOTES. Enter information not included elsewhere such as: prepared in cooperation with; translation of; report supersedes; old edition number, etc.

14. ABSTRACT. A brief (approximately 200 words) factual summary of the most significant information.

15. SUBJECT TERMS. Key words or phrases identifying major concepts in the report.

16. SECURITY CLASSIFICATION. Enter security classification in accordance with security classification regulations, e.g. U, C, S, etc. If this form contains classified information, stamp classification level on the top and bottom of this page.

17. LIMITATION OF ABSTRACT. This block must be completed to assign a distribution limitation to the abstract. Enter UU (Unclassified Unlimited) or SAR (Same as Report). An entry in this block is necessary if the abstract is to be limited.

Table of Contents

List of Tables

List of Figures

ABSTRACT

In this study, the microwave absorption characteristics of metallic glass / polymer composites were investigated. Electromagnetic wave absorption properties in the microwave spectrum are of particular importance to military applications. Radar absorbing materials have been studied for years and are of strategic importance for stealth technology. This work examined high magnetic permeability cobalt-based metallic glasses dispersed in epoxy matrices and measured the reflection loss behavior of the composites in the C-band and X-band spectrum. Results have shown that the metallic glass composites have good absorption in the region of interest due to the absorption properties of the glass particles and the graded structure of the composite.

BACKGROUND

Microwaves range in frequencies from 0.3GHz to 300 GHz, covering the EM spectrum from radio waves to far-infrared frequencies. X-band radar, for example, is in this spectrum and is between 8-12 GHz. Radar absorbing materials research began in the 1930's and continues to the present day. Lossy materials such as carbonyl iron and ferrites have been used in stealth technology as well as other electromagnetic shielding applications in general. Recently, there has been research to examine materials such as nano-particles, polymers, and other metamaterials. Radar absorbing materials work by reducing the amount of reflected energy to the radar by means of absorption processes. This can occur by the placement of dielectric or magnetic materials at the surface of the object which provides impedance to the incoming electromagnetic wave. The radar absorbing materials transfer the incoming EM energy into heat within the material. This type of material is classified as "lossy". The loss mechanisms are associated with the complex permittivity (ε) and the complex permeability (μ). These values are expressed by,

$$\varepsilon = \varepsilon' - i\varepsilon''$$
$$\mu = \mu' - i\mu''$$

where the real part (energy storage) is shown as a prime and the imaginary part (energy loss) is shown as a double prime. The loss in the material occurs when the microwave frequencies transfer energy to the atoms in the material and the molecular dipoles oscillate. The loss tangent is expressed as:

$$\tan\delta_e = \varepsilon''/\varepsilon'$$
$$\tan\delta_\mu = \mu''/\mu'$$

Metallic glasses, or amorphous metals, are essentially frozen liquids with amorphous atomic structure, e.g. no long range atomic order as would be seen in a crystalline material. Figure 1 shows an amorphous atomic arrangement on the left and a crystalline order on the right. These materials can have attractive properties such as high strength and modulus and interesting electrical and magnetic properties.

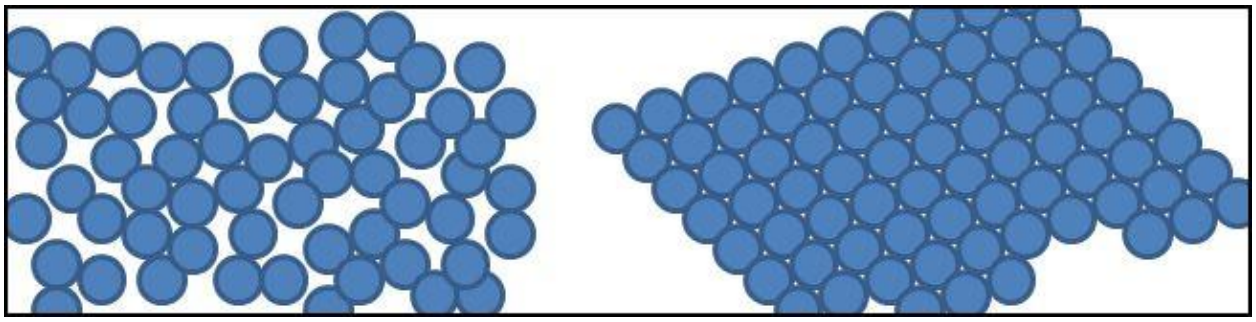

Figure 1: Atomic arrangement in a glass (left) and a crystal (right).

The interaction of microwaves with metallic glass has been studied, for scenarios such as heating and sintering [1, 2]. Metallic glasses have also been studied extensively due to their soft magnetic properties and applications for toroidal cores [3, 4]. As is the case in this current research, some have looked at metallic glasses in polymers [5, 6, 7]. In 1980 Kadir et al made composites of metallic glass ribbon and epoxy to examine the mechanical strength and observed good interfacial contact between the glass ribbons and the epoxy [6]. Powell et al investigated metallic glass in polymer paste for magnetic properties. MetGlas amorphous metal ribbon was annealed and high energy ball-milled into powders. Post-milling anneals below the glass crystallization temperature were used to develop superior magnetic properties and to reduce the internal stresses of the ribbon imparted during milling. This anneal improves the magnetic properties and can also be performed under magnetic fields in order to further increase the permeability of the material.

Materials like ferrites [8, 9, 10] and carbonyl iron have been traditionally used in radar absorbing applications. More recently, many types of materials have been examined for microwave absorption. Materials such as nanotubes and nanoparticles have been examined for their absorption properties [11, 12, 13, 14, 15, 16, 17]. Analytical models exist that describe composite materials that contain magnetic particles. These models can be used to predict the effective permeability of a composite [18]. The symmetrical Bruggeman's formula can be used for effective permeability of a mixture of randomly oriented ellipsoidal inclusions of intrinsic permeability μ_i in the background medium:

$$\boldsymbol{\mu_{eff} = \mu_b + \frac{v_i}{3}(\mu_i - \mu_b)\sum_{k=1}^{3}\frac{\mu_{eff}}{\mu_{eff} + N_k(\mu_i - \mu_{eff})}}$$

where v_i is the volume fraction of the magnetic inclusions, μ_b is the permeability of the background matrix, which may be non-magnetic (μ_b=1), and μ_i is the intrinsic permeability of the particles. Though this equation takes into account shape factors, the resultant μ_{eff} turns out to substantially overestimate realistic permeability obtained using the asymmetric Bruggeman's formula, or 1/3-power mixing rule, for spherical inclusions, which is:

$$\boldsymbol{\frac{\mu_i - \mu_{eff_i}}{\mu_i - \mu_b} = (1 - v_i)\left(\frac{\mu_{eff}}{\mu_b}\right)^{1/3}}$$

and μ_i is approximated to be $\mu_b/(1+\alpha\mu_b)$ for $\mu_b>>1$, where $\alpha=\delta/d$ and δ is the average gap between crushed magnetic particles and d is the average diameter of these pieces if all the particles were pressed into a solid and its intrinsic permeability was measured. This type of modeling analysis was intended for this project, however, due to difficulties in measuring the permeability of the composites, the analysis was not performed.

EXPERIMENTAL PROCEDURE

Two cobalt based metallic glasses were used in this project. The first composition was made from mechanical alloying of amorphous powders of cobalt, iron and silicon. The "powder to powder" materials were 85Co-10Si-5Fe (NanoAmor, Houston, TX) by weight. These powders had a density of approximately 6.88 g/cc. The second metallic glass composition was made from milling MetGlas 2714A (MetGlas, Conway, SC) metallic glass ribbon. This ribbon material had a nominal composition of 85Co-9Si-4Fe-1Ni-1B and a density of 7.59 g/cc. After milling/mechanical alloying was completed, the powders were annealed. The powders must be annealed after milling in order to relieve stresses incurred from the milling process and to enhance their magnetic properties. Careful attention must be given to the crystallization temperature so that the amorphous structure does not transform to the more stable crystalline atomic structure. The ribbon derived material was annealed at 400°C for 1 hour in vacuum and remained 99% amorphous. The annealing temperature for the powder derived material was determined to be 300°C. The material was consequently annealed for 1 hour in vacuum at this temperature with a final amorphous content between 70-90%. The final particle size distribution for the powder derived material was 2-25 microns and 2-50 microns for the ribbon derived material.

Epoxy was chosen as the polymeric matrix material for the metallic glass composites. Epoxy 2000 (Fibre Glast, Brookeville, OH) epoxy resin and hardener system was used for this study. Metallic glass powders were mixed with the resin and hardener in a Flacktek DAC 150 FVZ-K high shear mixer for 1 minute at 1000 rpm and 2 minutes at 2000 rpm. The mixed epoxy and powders were then degassed in a vacuum oven for 15 minutes and cast into silicone molds and cured overnight in a pressure chamber at 70 psi. Samples of neat epoxy, 5 and 15 vol% (24wt%, 52wt%) 85Co-10Si-5Fe, and 5 and 15 vol% (26wt%, 55wt%) 85Co-9Si-4Fe-1Ni-1B were made. The MetGlas derived samples (85Co-9Si-4Fe-1Ni-1B) were given the nomenclature M5 and M15 and the powder derived material (85Co-10Si-5Fe) were given the nomenclature P5 and P15. The samples had the dimensions $l = w = 1.5$ inches and a nominal thickness of 0.25 inch. The composites were post-cured at 90°C for 4 hours. The P15 and P15 samples had densities of 1.45 g/cc and 1.98 g/cc, respectively, and the M5 and M15 samples had densities of 1.48 g/cc and 2.09 g/cc, respectively. After the samples were machined for testing, the samples had the dimensions shown in Table 1. Examination of the fracture surface showed no signs of porosity.

	PROJECT: 1022		
Material	L (in)	W (in)	H (in)
X-band			
P5	0.90133	0.40038	0.26087
P15	0.90192	0.40013	0.25427
M5	0.90197	0.40032	0.23352
M15	0.90128	0.40067	0.25405
Epoxy	0.90110	0.40062	0.24603
C-band			
P5	1.365	0.62310	0.24692
P15	1.368	0.62195	0.23320
M5	1.337	0.62343	0.22757
M15	1.364	0.62350	0.23498
Epoxy	1.370	0.62375	0.23873

Table 1: Dimensions of samples for testing.

Tests at AFRL (Berrie Hill Corporation)

The test setup for a generic waveguide is shown in Figure 2. Since the desired range to be measured was 5 – 12.4 GHz, two waveguide systems had to be used. The high C-band waveguide covered the range of 5 – 8.2 and the X-band waveguide covered 8.2 – 12.4 GHz. When using the waveguide system to determine material parameters, the material is placed in the waveguide and the scattering parameters (refl – S11, S22, trans – S21, S12) are measured. Figure 2 shows a generic waveguide system.

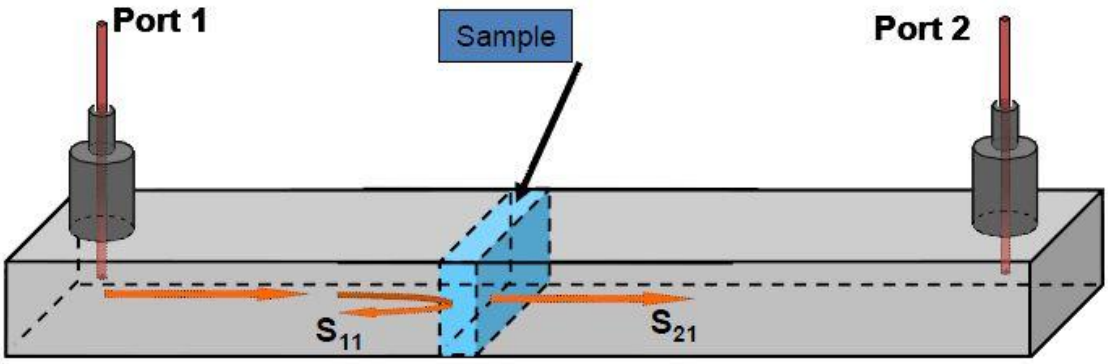

Figure 2: Generic rectangular waveguide system.

An Agilent E8361A Programmable Network Analyzer (PNA) was used to record the data. The settings for the PNA are shown in Table 2. A second series of measurements was taken with a metal short next to the sample holder. Only the S11 parameters were measured for these, as the rest of the parameters are meaningless. This second series of measurements allow us to find an absorption curve for the materials over the desired frequencies. Both sides of each sample were measured using this test configuration, as seen in Figure 3, as an incoming wave will behave differently depending on the side of the inhomogeneous material it approaches. The epoxy sample only needed one side of the metal-backed test to be performed since it is a homogeneous material.

Averaging	Off
Port output power	-10 dBm
Intermediate Freq BW	300 Hz
Number of data points	801
Sweep type	Stepped frequency, 0 ms dwell time
System Z_0	1 Ω
Calibration type	TRL

Table 2: Network analyzer settings.

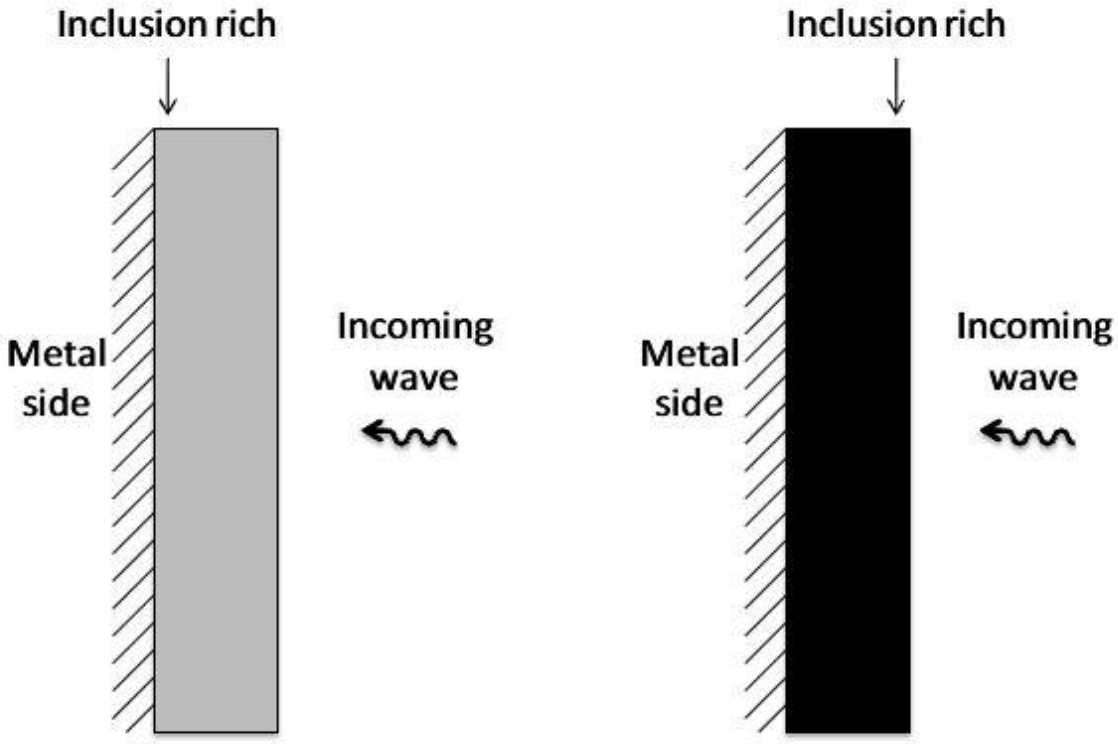

Figure 3: Diagram of the two orientations for metal backed test.

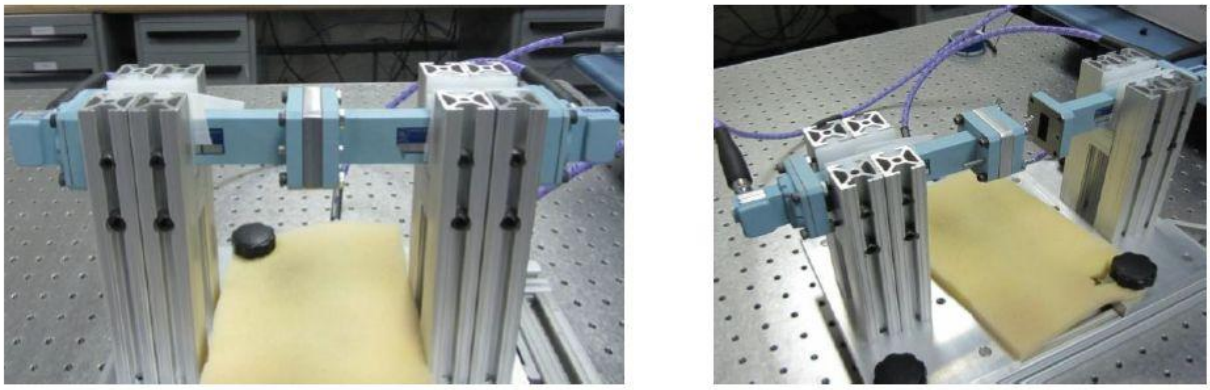

Figure 4: Rectangular X-band waveguide setup (left) and metal backed test setup (right).

The X-band waveguide setup is seen in Figure 4. The waveguide is held by a sliding metal bracket that can be locked down while the sample holder is inserted or removed. The metal bracket helps reduce the amount of cable motion during the testing process, reducing the amount of error created. The C-band waveguide system was also put into the metal bracket while those samples were being tested. During this test the inclusion rich side of the sample was placed in the sample holder facing toward Port 1. Figure 4 shows the X-band metal backed testing setup. The sample is placed in the sample holder such that one side of the sample is juxtaposed with the

metal reflection standard. The C-band and X-band sample holders are shown in Figure 5 and the actual samples are shown in Figure 6.

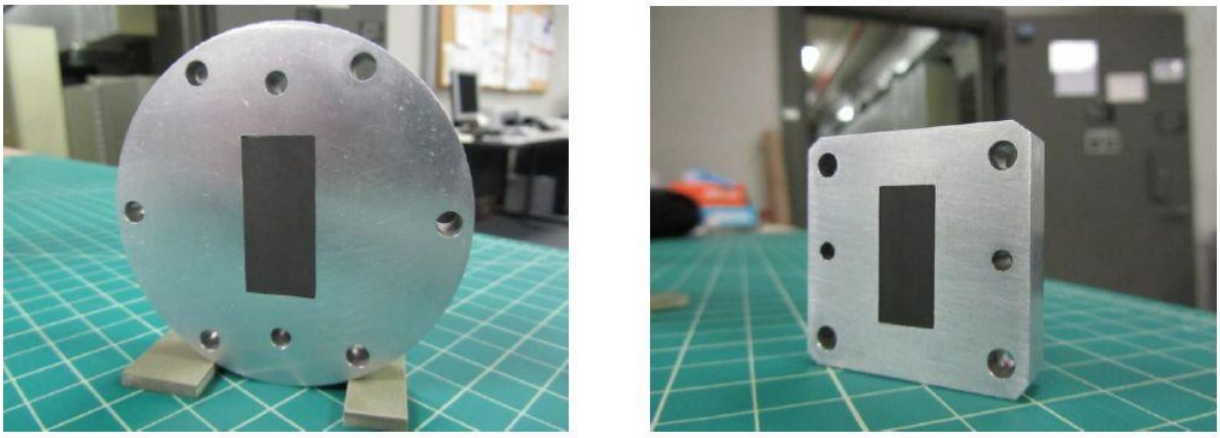

Figure 5: Samples in c-band set-up (left) and x-band set-up (right).

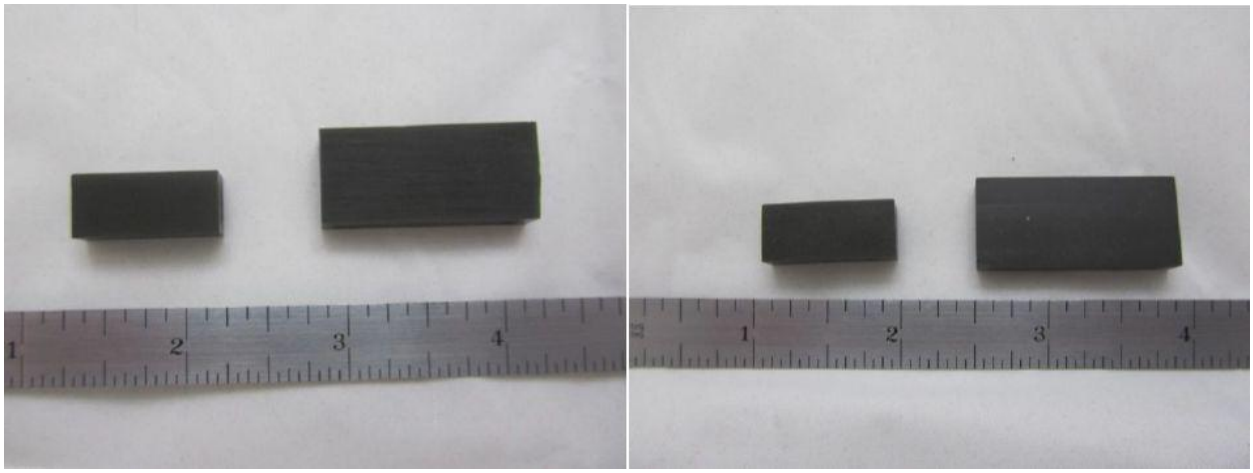

Figure 6: An example of the actual test samples (P5 and P15).

RESULTS

Material Microstructure

Figures 7 and 8 show the starting powders of the MetGlas ribbon derived powders and the powder derived material. The MetGlas derived powder had a higher average particle size as compared to the powder derived material as can be seen in the scanning electron micrographs. Figures 9 and 10 show the x-ray diffraction results after annealing the post-milled powders at 400°C for 1 hr. The ribbon derived powder (Figure 9) responded well and was 99% amorphous.

The powder derived material had increased nano-crystallinity compared to the original material. The annealing temperature for the powder derived material was lowered to 300°C and had a final nano-crystallinity content between 10-30%. Remnant mixed epoxy and powder for each material composition was cured and cryo-fractured and viewed in the electron microscope for dispersion quality. Figure 11 shows a 5 vol% sample of the MetGlas composite and Figure 12 shows a 15 vol% composite. The metallic glass particles are clearly seen embedded in the epoxy matrix, with a higher density of particles seen in the 15 vol% composite.

a)

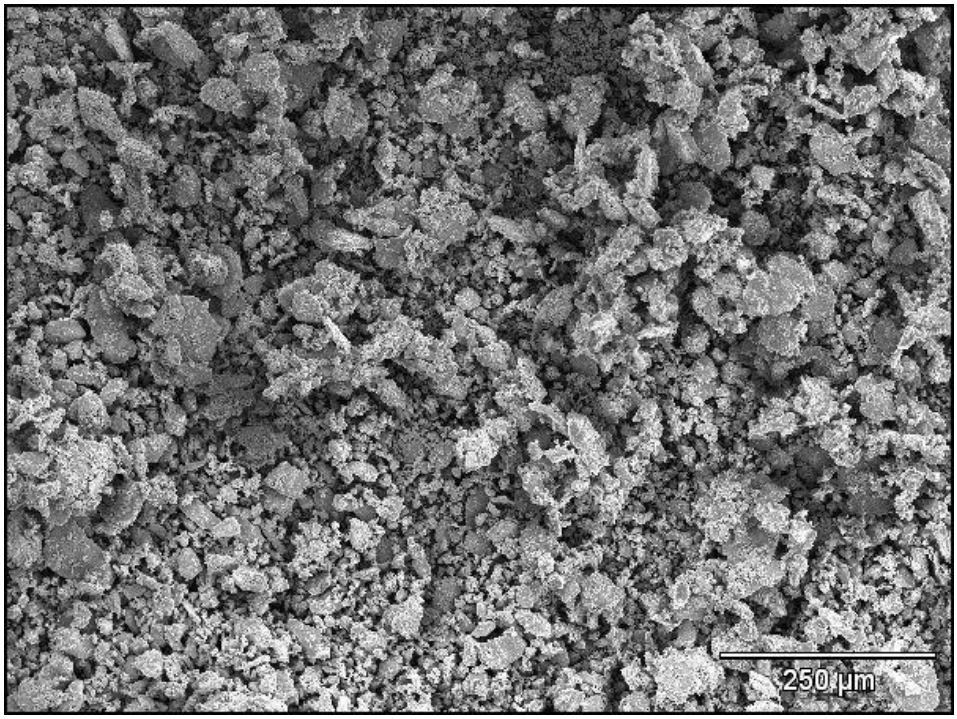

b)

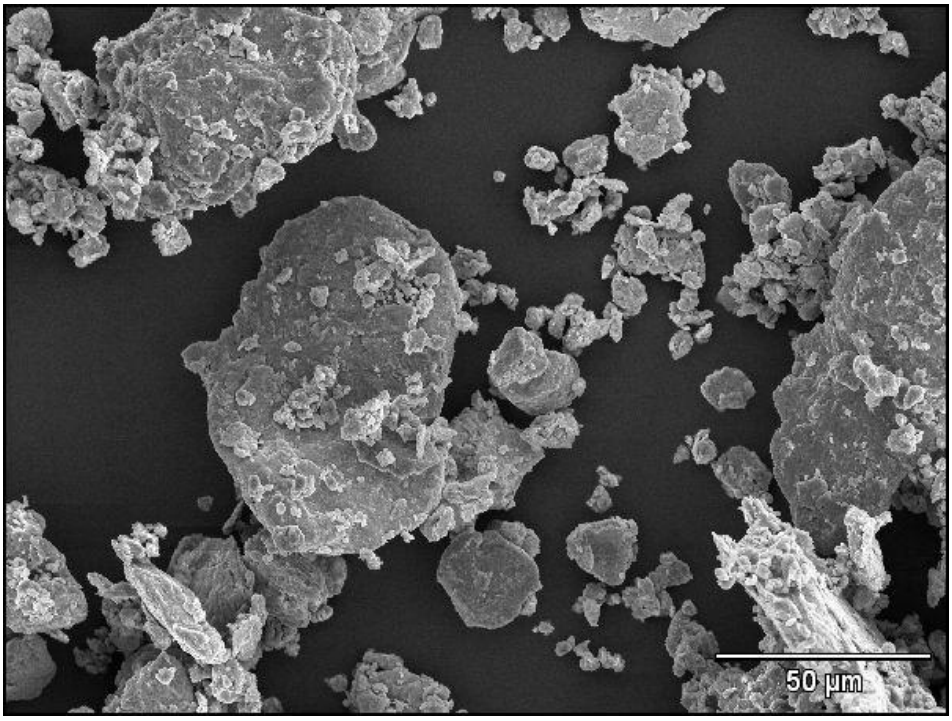

Figure 7: MetGlas ribbon derived powders a) low magnification and b) high magnification.

a)

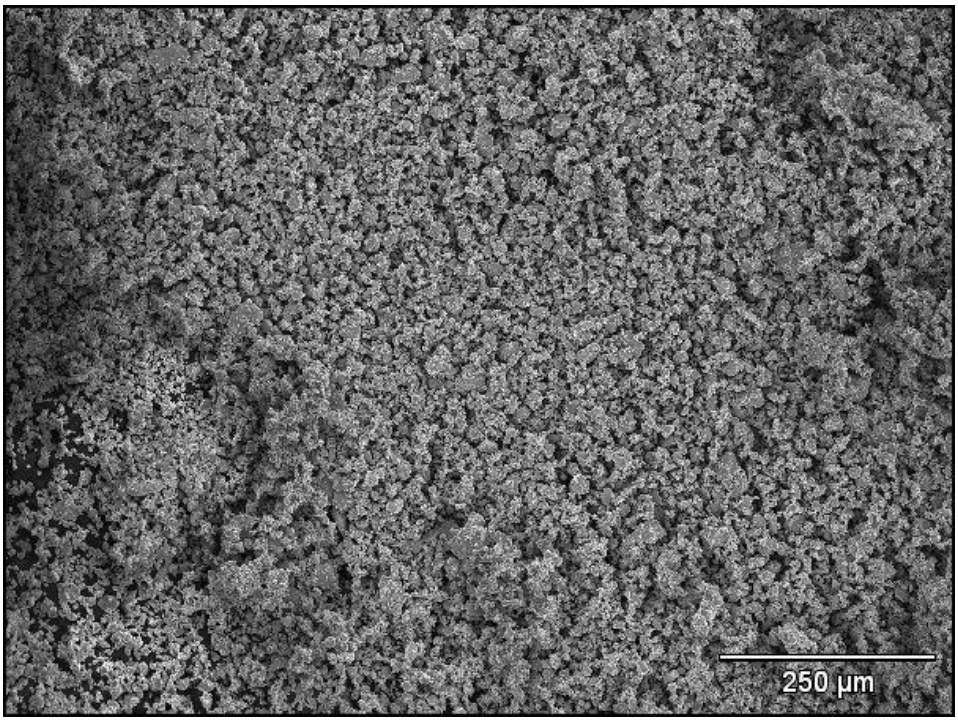

b)

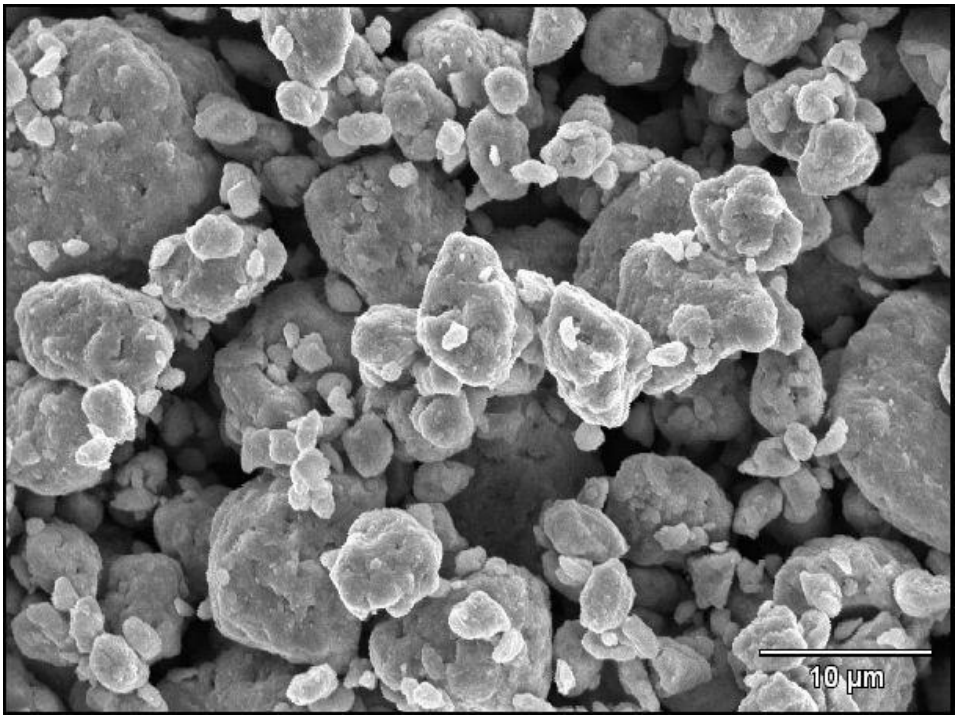

Figure 8: Powder derived powders a) low magnification and b) high magnification.

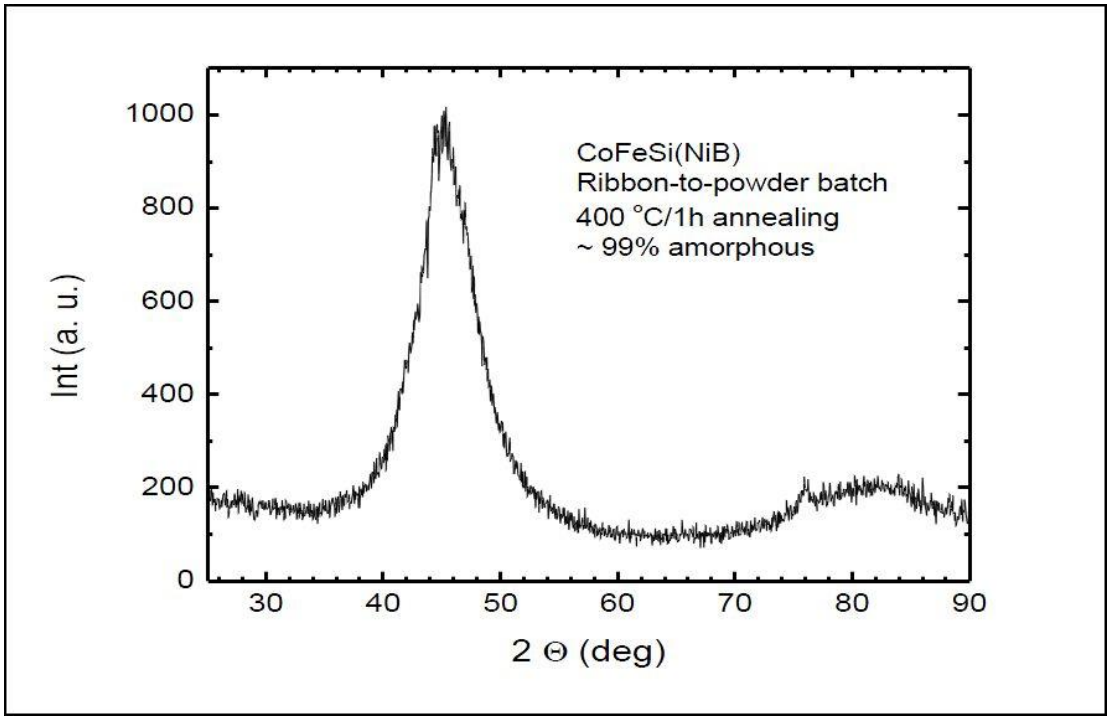

Figure 9: XRD of the post-annealed ribbon derived powder.

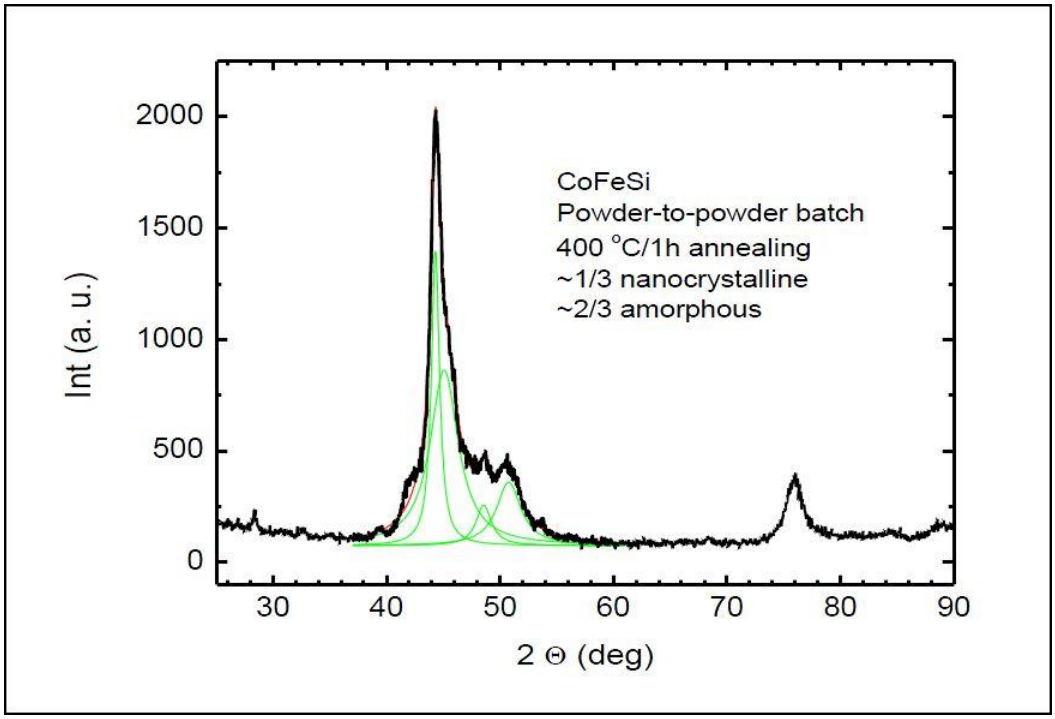

Figure 10: XRD of the post-annealed powder derived powder. Subsequent annealing was changed to 300C.

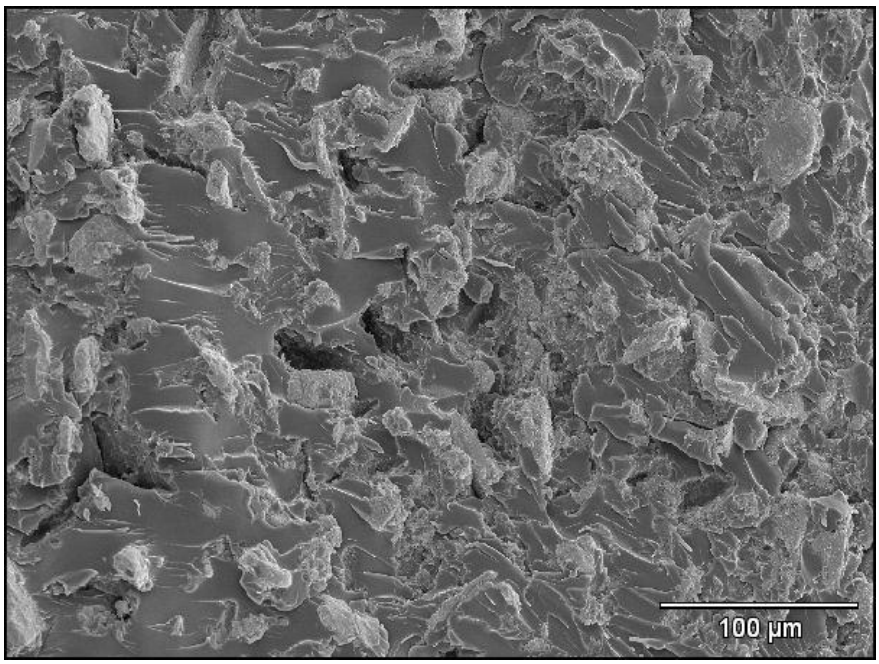

Figure 11: Fracture surface of 5 vol% MetGlas powder composite.

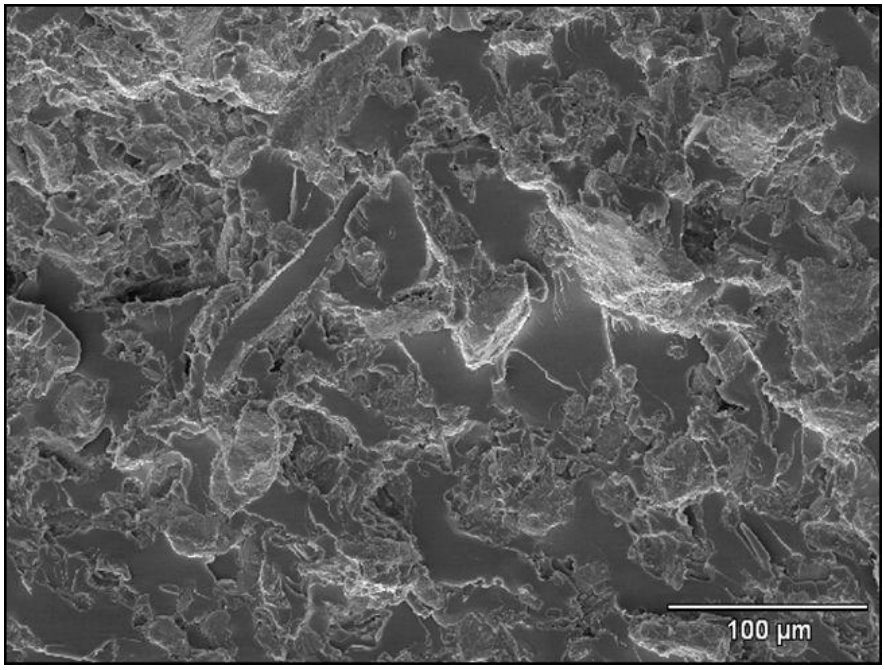

Figure 12: Fracture surface of 15 vol% MetGlas powder composite.

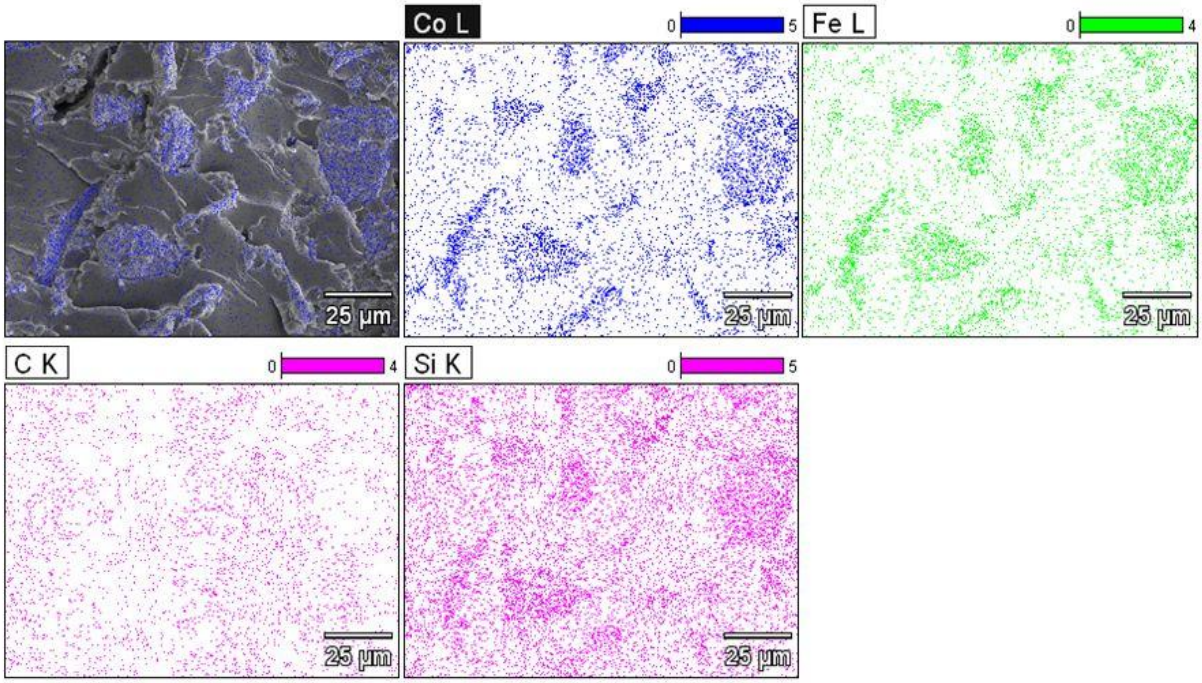

Figure 13: EDS map of 5 vol% composite showing location of the metallic glass particles. The Fe spectra is superimposed on the SEM micrograph.

Energy Dispersive Spectroscopy was used to map the major elements of the metallic glass particles embedded in the epoxy matrix. The glass particles are clearly differentiated on the fracture surface when the EDS map for iron is superimposed on the SEM micrograph. The EDS maps for Co, Si and Fe all coincide with each other on the location of the metallic glass particles in Figure 13. While viewing the fracture surfaces in the electron microscope it was observed that the lower region of the fracture surface had a higher density of metallic glass particles, while the top portion was relatively void of the material (Figure 14). This figure clearly shows a very well functionally graded material with higher metallic particle concentration on the bottom of the sample (relative to how it was oriented during curing) and lower concentration at the top. It appears the larger, heavier particles settled to the bottom and smaller particles experienced less settling, as one would expect to see in a viscous fluid. Based on a visual inspection, the volume fraction of particles on the inclusion rich side of the composite is likely to be between 30-50%. The specific gravity of the epoxy is 1.12 g/cc and the densities of the MetGlas powder and Powder derived powder are 7.59 g/cc and 6.88g/cc, respectively. The epoxy viscosity was approximately 950 cps. A lower viscosity epoxy combined with dense glass particles likely resulted in significant settling of the particles during the first few hours of curing. For this reason, reflection loss measurements were made on both sides of the sample. The interface between the glass particles and the epoxy resin is seen in Figure 15. There appears to be small gaps between the particle and matrix indicating poor interfacial bonding. This has been reported previously in the literature [6].

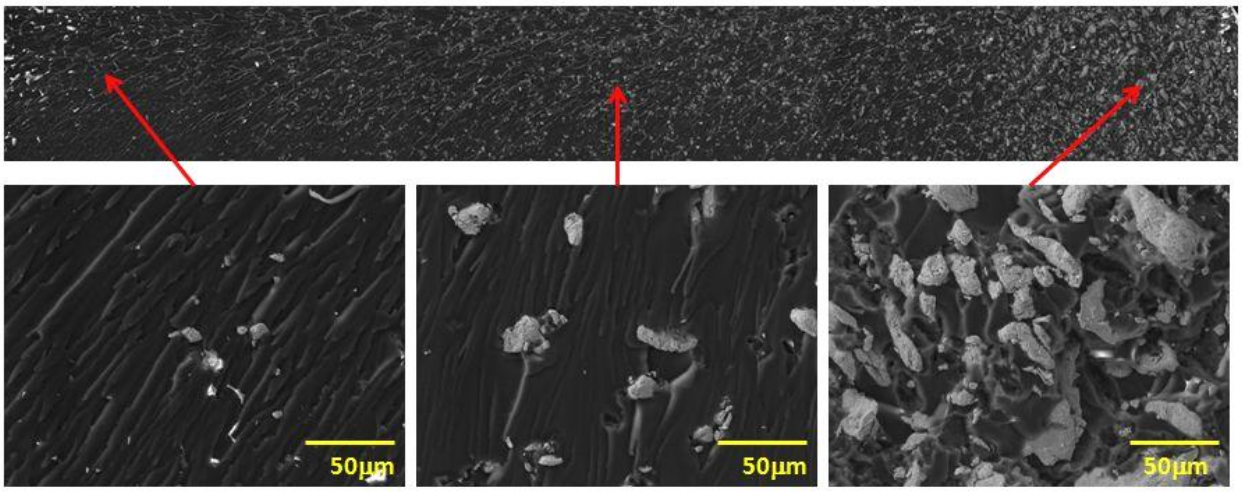

Figure 14: Fracture surface of 15vol% MetGlas (Sample M15) showing settling of particles towards bottom (right) of specimen. The top portion of the figure is entire cross section of the M15 sample. The bottom three micrographs show higher magnification of the top, middle, and bottom of the sample clearly showing the difference in particle content.

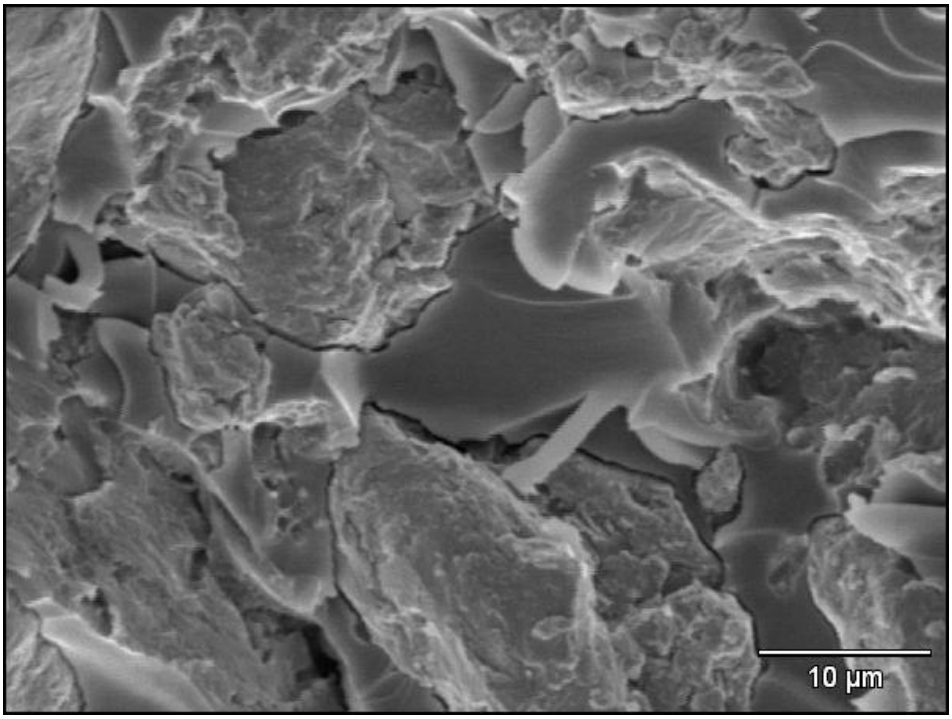

Figure 15: Metallic glass particles in MetGlas composite showing poor interface between filler and matrix.

Results of Absorption Testing

The results of the scattering measurements and the |S11| measurements from the metal-backed experiments are shown in the following data sets.

Figures 16-20 show the scattering parameters for both C- and X-band samples for each material. Evidence of the inhomogeneity of the samples can be seen in the figures. If the sample was homogeneous the |S11| and |S22| values would be equal. The difference implies that the plane wave is interacting with two different material faces, one being more reflective than the other. The higher the magnitude of |S11| or |S22| signifies a higher reflectivity of that face (recalling that the inclusion rich side is facing Port 1). The homogeneous pure epoxy sample did not display this behavior.

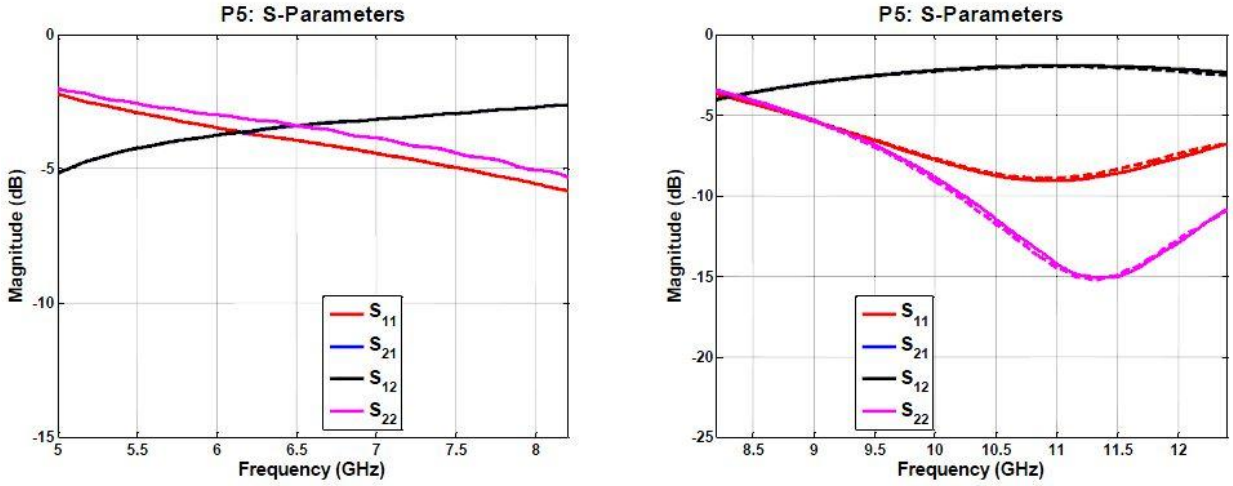

Figure 16: C-band and X-band scattering parameters for P5 material.

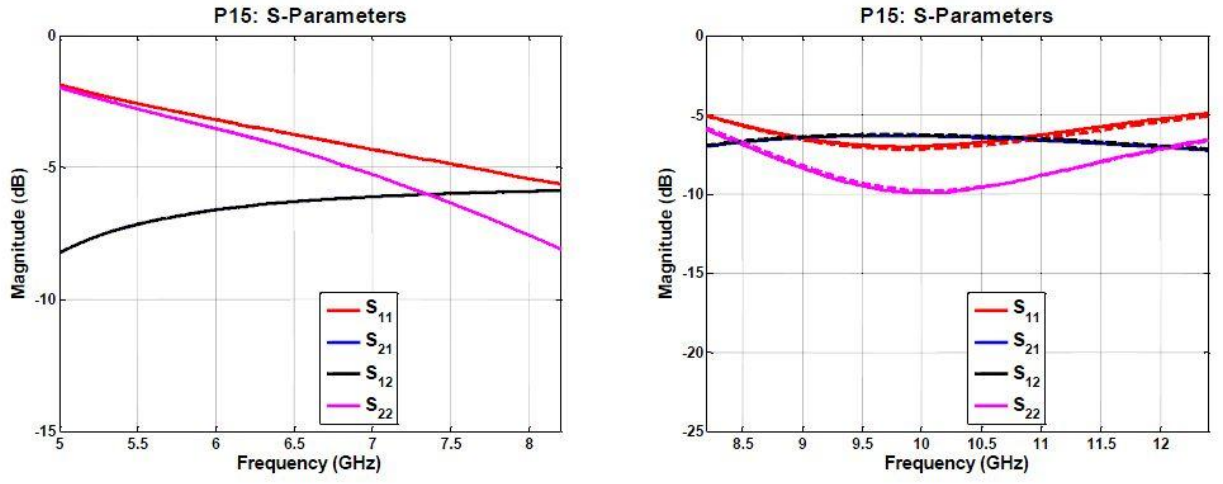

Figure 17: C-band and X-band scattering parameters for P15 material.

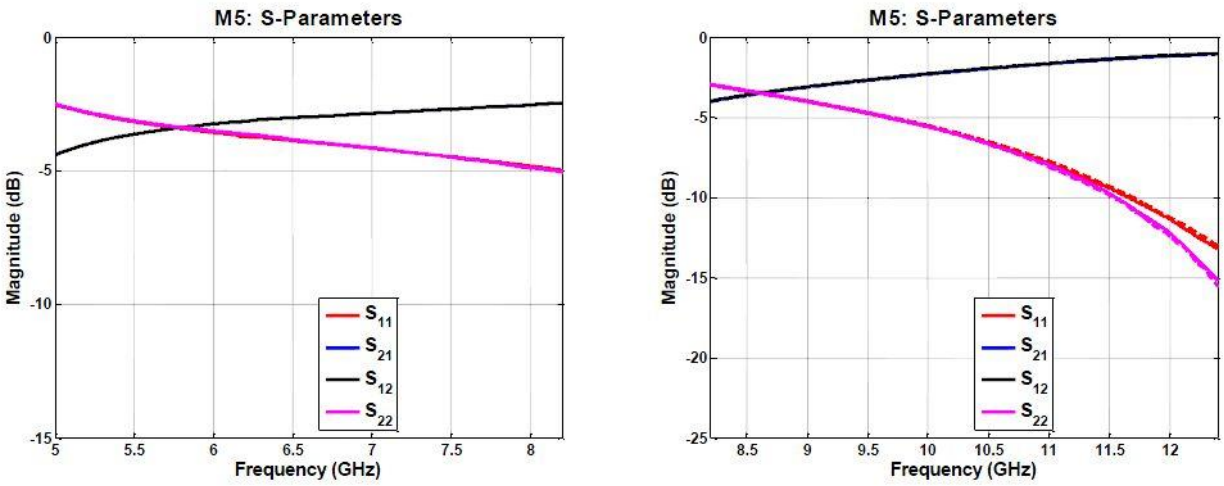

Figure 18: C-band and X-band scattering parameters for M5 material.

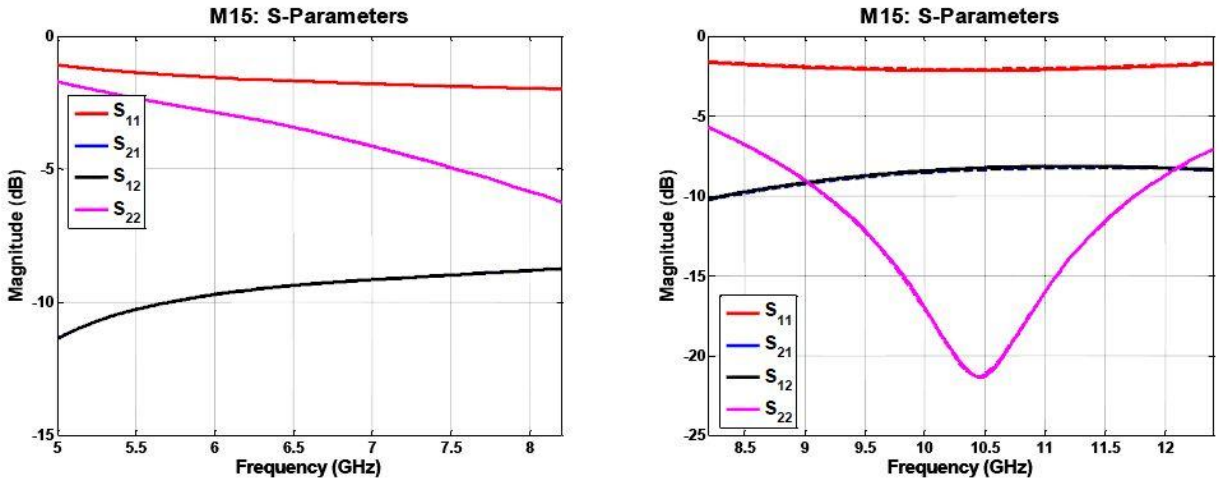

Figure 19: C-band and X-band scattering parameters for M15 material.

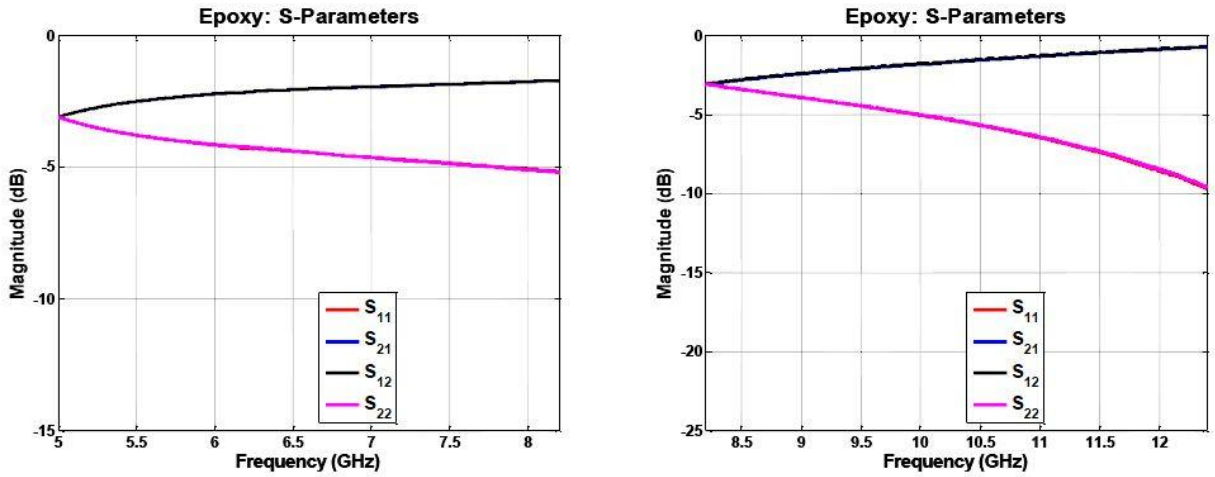

Figure 20: C-band and X-band scattering parameters for pure epoxy material.

Figure 21 through Figure 25 show the measurements for the metal backed experiment. The plots on the left side show the results when the inclusion rich side was placed next to the metal backing and the right side plots display the results when the inclusion deficit side of the material was placed next to the reflection standard. Generally, the inclusion rich side against the reflection standard had higher absorption. This shows that the inclusion rich side is reflecting more of the signal before the wave enters the material. This is due to the higher impedance change from air to the inclusion rich side.

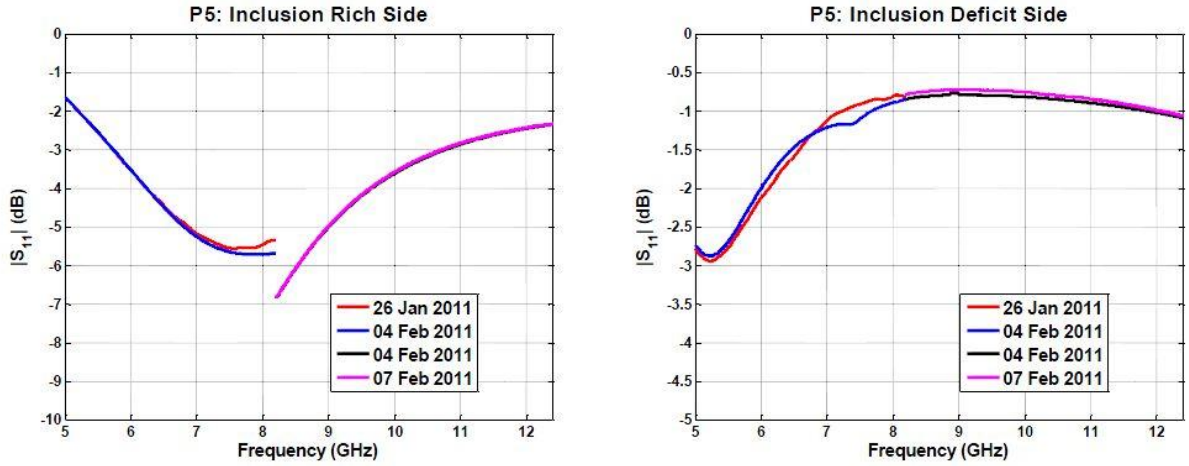

Figure 21: C-band and X-band metal backed S11 for P5 material.

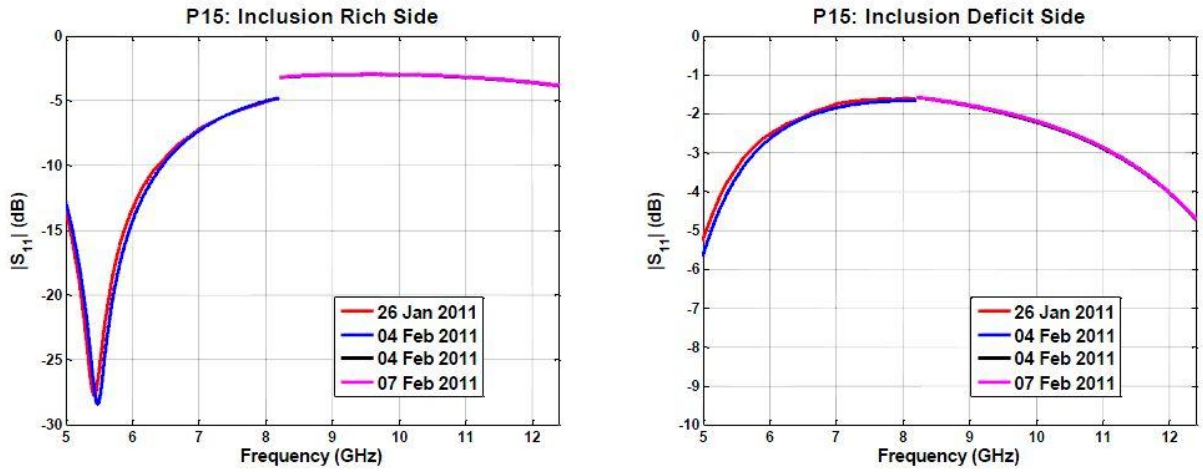

Figure 22: C-band and X-band metal backed S11 for P15 material.

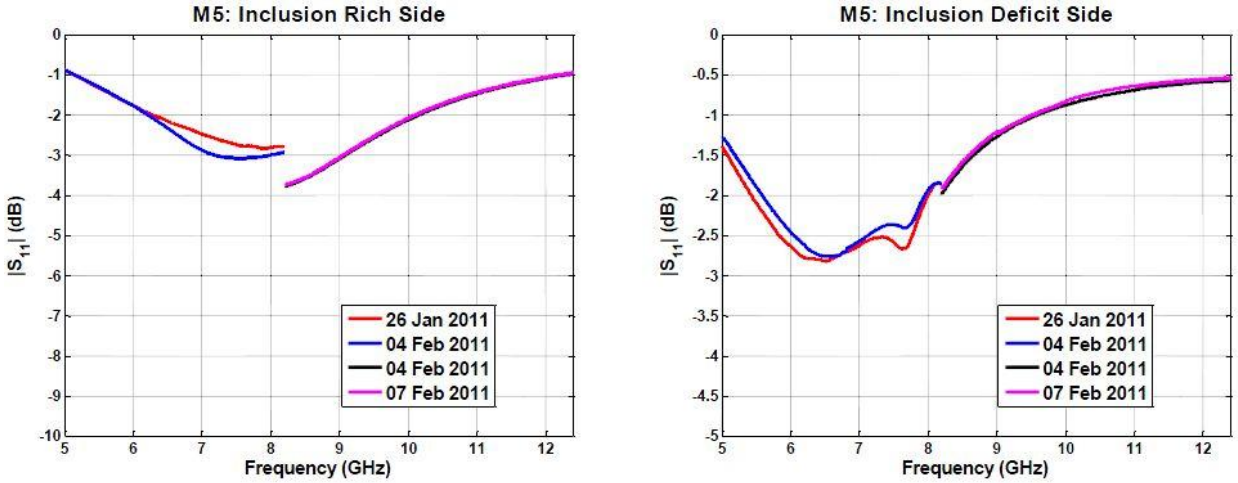

Figure 23: C-band and X-band metal backed S11 for M5 material.

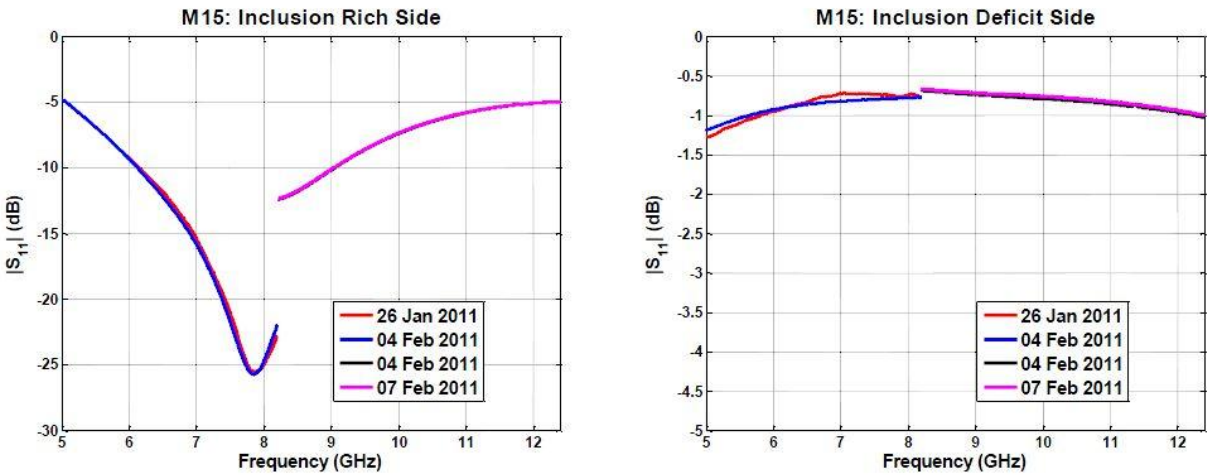

Figure 24: C-band and X-band metal backed S11 for M15 material.

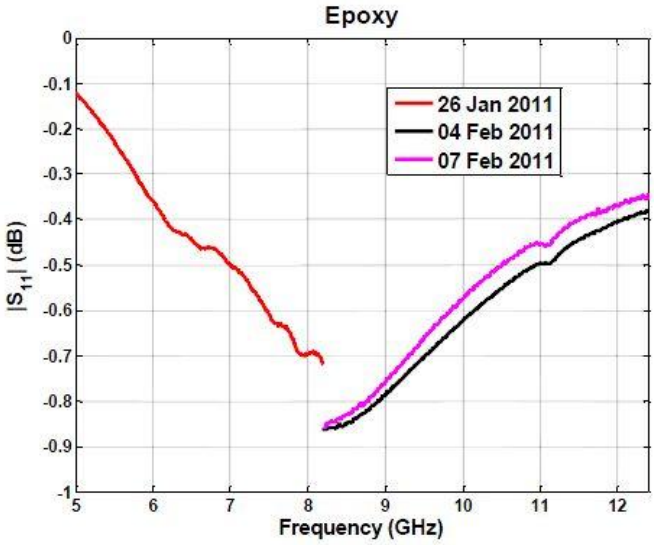

Figure 25: C-band and X-band metal backed S11 for pure epoxy material.

DISCUSSION

The first set of experiments confirmed that all the samples with inclusions were not homogeneous, as the S11 and S22 parameters were not equal. The first set of the experiments also showed which side of the material was more reflective. The second set of experiments (metal backed) showed the absorption for each of the materials. The inclusion rich side against the reflection standard generally showed higher absorption than when the deficit rich side was against the absorption standard.

Based on the results of the absorption tests, it is clear that the metallic glass particles absorb the electromagnetic waves in the region of interest. A comparison of the two compositionally differing powders shows that the P15 and M15 samples absorbed the most, with peak absorption

between -25dB and -30dB. The M15 material tended to absorb at slightly higher frequency than the P15 material, with peak absorptions for each material at 7.8 GHz and 5.5 GHz, respectively. The P15 material showed good broadband absorption (greater than -10dB) from 4.5 GHz (estimation based on extrapolation) to 6.5 GHz and the M15 showed good broadband absorption over most of the C-band and part of the X-band region tested (6-9 GHz). In this range, the material can achieve 90% reflection loss [14]. It is clear from the data that volume fraction of powder had a larger effect on absorption performance than the slightly differing chemistries of the two powders used. Both chemistries have absorption peaks between -25dB and -30dB. It is not known if the slight chemistry differences and crystallinity differences between the two powders lead to any of the observed differences in absorption behavior. If the factors did contribute to the differences, they appear to be small based on the data.

Due to the in-homogeneity of the samples, the complex permeability and permittivity tests were not able to be conducted. This data would have been helpful to have in order to see how the metallic glass particles affect permittivity and permeability of the composite. One interesting result seen in the absorption tests is that the inclusion rich side against the metal plate showed higher absorption than when the inclusion rich side was away from the metal plate. This is likely due to the gradual difference in impedance as the wave traverses the graded composite material. Increased absorption may be an unintended, but welcomed, consequence of the metallic glass particles settling during composite preparation. The inadvertent formation of this functionally graded composite seems to have lead to a better performing material. It is difficult to extract how a homogeneous sample of this composite would behave in similar testing. The graded composites in this study performed similarly to materials that performed well in other results presented in the literature [11, 13, 14, 15]. It is also difficult to correlate the results in these waveguide tests to how the material might behave in a free space experiment, such as an anechoic chamber reflection experiment.

Future work in this area should investigate how a homogeneous material behaves in comparison to a graded material. Other aspects that could be investigated are alternate metallic glass and polymer compositions, differing weight fractions, and thorough permittivity and permeability testing. Once optimized, these materials could provide the basis for radar absorbing composites, particularly where weight is not an issue, due to the high densities of cobalt-based metallic glasses.

SUMMARY

High permeability cobalt-based metallic glass powders were fabricated and blended with epoxy to form composite structures. Microstructural characterization of the composites showed that the metallic glass particles settled during curing, forming a functionally graded microstructure. The samples were then tested for S-Parameter scattering parameters and absorption properties using a waveguide and network analyzer. The results showed that the electromagnetic scattering and absorption properties in the upper C-band and X-band spectrum were dependent upon the metallic glass content at the surface. S11 scattering/absorption results showed increased scattering from the inclusion-rich side due to high impedance changes. There was increased absorption when the inclusion-rich side was placed next to the metal plate standard. Composites with higher metallic glass content achieved larger absorption levels (greater than -25 dB). The

M15 material achieved greater than 90% broadband absorption in the upper C-band and X-band spectrum, 6 GHz to 9 GHz, while the P15 material achieved great than 90% absorption from 4.5 GHz(est) to 6.5 GHz.

REFERENCES

1. D.V. Louzguine-Luzgin, G.Q. Xie, S. Li, A. Inoue, N. Yoshikawa, K. Mashiko, S. Taniguchi, M. Sato, J. of Alloys and Compounds, Volume 483, Issues 1-2, 26 August (2009) 78-81.
2. G. Xie, S. Li, D.V. Louzguine-Luzgin, Z.Cao, N. Yoshikawa, M. Sato, A. Inoue, Proceedings of the 13th International Conference on Rapidly Quenched and Metastable Materials, Journal of Physics: Conference Series 144 (2009), 012049.
3. H-Y. Chang, P-C. Yao, D-R. Huang, S-E. Hsu, Mat. Res. Soc. Symp. Proc., Vol 80, (1987) 423-428.
4. A. Makino, T. Hatanai, A. Inoue, T. Masumoto, Mat. Sci. Eng. A, Vol 226-228, (1997) 594-602.
5. L.K. Powell, I.Z. Rahman, M.A. Rahman, C. O'Mathuna, S. O'Reilly, J. of Mat. Proc. Tech., 119 (2001) 318-323.
6. W. Kadir, C. Hayzelden, B. Cantor, J. of Mat Sci Letters, 15 (1980) 2663-2664.
7. S. Li, D.V. Louzguine-Luzgin, G. Xie, M. Sato, A. Inoue, Materials Letters, 64, (2010) 235-238.
8. Y. Naito and K. Suetake, IEEE Trans. MTT-19, Jan (1971) 65-72
9. A. Verma, R. G. Mendiratta, T.C. Goel, D.C. Dube, Journal of Electroceramics, 8, (2002) 203-208.
10. M.R. Meshram, N.K. Agrawal, B. Sinha, P.S. Misra, J. of Magnetism and Magnetic Materials, 271, (2004) 207-214.
11. Z. Fan, G. Luo, Z. Zhang, Li Zhou, F. Wei, Mat. Sci. and Eng. B, 132 (2006) 85-89.
12. J.A . Roberts, T. Imholt, Z. Ye, C.A. Dyke, D.W. Price, J.M. Tour, J. Appl. Phys. **95**, 4352 (2004).
13. K-Y. Park, J-H. Han, S-B. Lee, J-B Kim, J-W. Yi, S-K. Lee, Comp. Sci. Tech., 69 (2009) 1271-1278.
14. J-H. Oh, K-S. Oh, C-G. Kim, C-S. Hong, Composite: Part B, 35 (2004) 49-56.
15. Y.L. Cheng, J.M. Dai, X.B. Zhu, D. J. Wu, Z.R. Yang, Y.P. Sun, Nanoscale Res Lett, DOI 10.1007/s11671-009-9374-y (2009).
16. V. Bregar, IEEE Trans. Magn., Vol 40, (2004) 1679-1684.
17. D. Micheli, C. Apollo, R. Pastore, M. Marchetti, Comp. Sci. Tech., Vol 70, Issue 2, (2010) 400-409.

18. M. Y. Koledintseva, J.L. Drewniak, Y. He, B. Matlin, Kyoto 2009 EMC Symposium, Japan, Paper 24P3-4, (2009) 809-812.